

Energetics of marine turbine arrays – extraction, dissipation and diminution*

Takafumi Nishino and Richard H. J. Willden

Department of Engineering Science, University of Oxford, Parks Road, Oxford OX1 3PJ, UK

ABSTRACT

A two-scale modelling approach is discussed to predict the performance and energetics of a large number (more than a few hundred) of marine turbines installed as a power farm in a general coastal environment. The kernel of this approach is that the outer, or coastal-scale, model/simulation is to assess the reduction of flow passing through a given farm area as a function of the increase of head loss across the farm, whereas the inner, or device-scale, model/simulation employs this function to account for the (otherwise unknown) effect of coastal dynamics for that farm site, i.e. diminution of the power removed from the farm area due to the reduction of flow through the farm. Large-eddy simulations (LES) of periodic open channel flow (with a porous plate model representing turbines) are then presented as a device-scale part of such a two-scale model of large marine turbine arrays. Results demonstrate the usefulness of this approach to study how the overall energetics of turbine arrays (i.e. extraction, dissipation and diminution of energy within the entire farm area) may change depending on the characteristics of the farm site, array configuration and operating conditions of the turbines in the farm.

Keywords: Tidal stream energy, Ocean current energy, Resource assessment, Numerical modelling, Large-eddy simulation

* This is an extended and revised version of a paper presented at the International Symposium on Marine and Offshore Renewable Energy, Tokyo, Japan, October 2013.

E-mail address: takafumi.nishino@eng.ox.ac.uk

34 **1. Introduction**

35 One of the key issues in the development of tidal- and ocean-current power generation
36 systems is to understand properly their prospective performance characteristics, not only for
37 each power generation device but also for device arrays or farms as a whole. This is
38 important for assessing the maximum power extractable from the ocean as well as for
39 optimising the configuration of the arrays or farms. Their performance is often described,
40 especially from a viewpoint of device developers, in terms of the power extracted by the
41 devices as useful power relative to either: (i) ‘available’ kinetic power (i.e. the kinetic power
42 of upstream flow through the frontal-projected area of devices); or (ii) power removed from
43 the flow (i.e. sum of that extracted as useful power and that dissipated into heat). When
44 deploying a large number of devices as a farm, however, we need to consider that the flow
45 through the entire farm area may reduce (due to very-large-scale flow deflection, for
46 example) and therefore both (i) available kinetic power and (ii) power removed from the flow
47 in that farm area may diminish substantially.

48 The importance of the reduction of flow through tidal arrays or farms has been
49 discussed in recent theoretical studies, but from a few different viewpoints. Garrett and
50 Cummins [1] considered an ideal power-extracting fence blocking an entire cross-section of a
51 tidal channel (i.e. neglecting the dissipation of energy due to wake mixing) and derived an
52 analytical model describing the relationship between the flow reduction and the power
53 extracted (for a given head difference across the channel). Vennell [2-4] combined the same
54 type of tidal channel dynamics model with a ‘confined flow’ version of the actuator disk
55 theory [5-7], thereby examined the optimal channel-flow reduction to maximise the power of
56 a number of devices arrayed regularly across the entire channel span (with gaps between each
57 device; i.e. taking account of the dissipation of energy due to device-scale wake mixing).
58 Meanwhile, Nishino and Willden [8, 9] considered an array of devices installed only across
59 part of the channel span (so that the channel flow may bypass the entire array) and derived a
60 ‘two-scale’ confined flow version of the actuator disk theory (i.e. considering the dissipation
61 of energy due to both device- and array-scale wake mixing). Although in [8, 9] the channel
62 inflow (rather than the head difference across the channel) was held constant to ignore the
63 channel dynamics effects, again the reduction of flow through the array area played a key
64 role in determining the conditions to maximise the power extracted.

65 These analytical models described above are all useful for understanding the basic
66 mechanisms that govern the performance characteristics of tidal arrays/farms in an ideal tidal

67 channel situation. When considering marine turbine arrays/farms in more general coastal
68 environments, however, it seems very difficult to predict their performance analytically. It
69 should be noted that, although the ‘partial array’ model of Nishino and Willden [8, 9] is
70 conceptually applicable to general coastal areas that are exposed to the open sea (by
71 considering zero or very low global blockage ratios), this model still needs to be combined
72 with a kind of ‘coastal dynamics’ model that properly accounts for the effects of seabed
73 friction and flow inertia across the entire area of interest. Since these effects depend
74 significantly on site-specific conditions (bathymetric features etc.) and are very difficult to
75 model analytically, we usually need to rely on numerical simulations of the shallow-water
76 equations; see e.g. Adcock et al. [10]. Three-dimensional Navier-Stokes simulations are, at
77 the present time, computationally very expensive and impractical for such geographic-scale
78 flow simulations.

79 Regardless of whether we model the coastal dynamics analytically or numerically (to
80 be combined with a model of power-extracting devices, which may also be either analytical
81 or numerical), one important question to be answered is if — and if so, how — we should
82 account for the interaction of (essentially three-dimensional) device-scale dynamics and
83 (approximately two-dimensional) coastal dynamics. For example, a large number of devices
84 densely deployed as a farm could change the vertical shear of the mean flow and thereby
85 change the bed friction *coefficient* (as well as the bed friction itself) across the entire farm
86 area, depending on the array configuration as well as operating conditions of devices within
87 the farm [11]. Note that if the friction coefficient changes then the power generation
88 characteristics of that farm area also change (as if the seabed in that farm area was changed
89 physically by adding or removing rocks etc.). Could such interaction be important for the
90 performance of turbine arrays? If so, how should we combine a three-dimensional device-
91 scale flow model/simulation with a two-dimensional coastal dynamics model/simulation to
92 account for the effects of such interaction?

93 In this study, we discuss a two-scale modelling approach to understand/predict the
94 performance of a large number (more than a few hundred) of marine turbines deployed as a
95 farm in a general coastal environment. The outline of the two-scale approach, which is a
96 combined device-scale and coastal-scale simulation, is described first in Section 2, followed
97 by an example of the device-scale part of the approach (LES of periodic open channel flow
98 with simplified device models) in Section 3. By using the results of LES (together with a
99 model function representing hypothetical coastal-scale simulation results), in Section 4 we

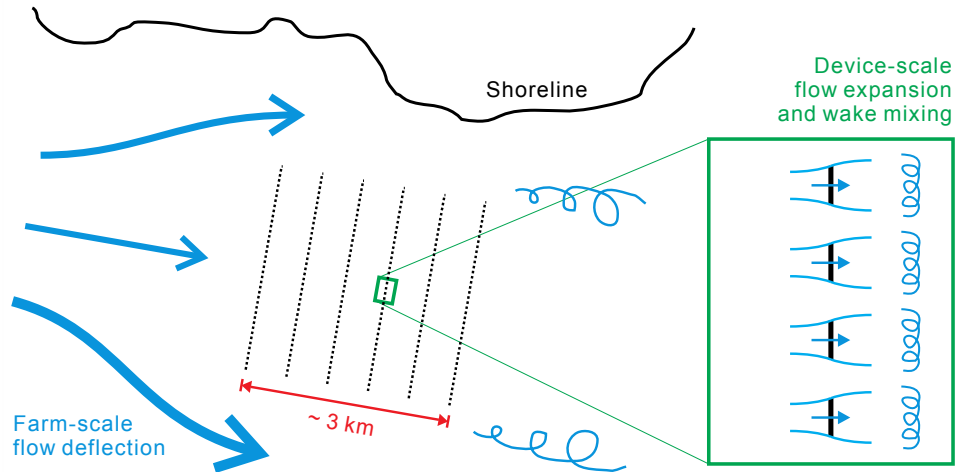


Fig. 1. Schematic of an example of coastal flow past a number (several hundred) of marine turbines.

100 demonstrate how the two-scale approach would work to understand/predict the performance
 101 and energetics of large turbine arrays as a farm (i.e., extraction, dissipation and diminution of
 102 energy within the farm area). Finally, conclusions are given in Section 5.

103

104 2. Outline of the two-scale modelling of marine turbine arrays

105 Let us consider a large number (several hundred) of marine turbines regularly arrayed as a
 106 farm, as shown in Fig. 1. For the sake of convenience, we consider the size of each turbine to
 107 be about 20m (common size for megawatt class turbines) and that all turbines are deployed
 108 within a few kilometre square ‘farm area’. This seems a possible scenario, considering that
 109 the farm needs to co-exist with other coastal activities, such as shipping and fishing. The
 110 front and rear edges of the farm area are perpendicular to a quasi-steady ocean current.

111 In order to make the two-scale modelling feasible, we assume that the seabed is (at
 112 least approximately) flat across the entire farm area. In addition, we assume that all turbines
 113 in the farm operate under approximately the same local flow conditions; hence the ‘locally-
 114 averaged’ streamwise velocity (i.e. velocity averaged across each segment or portion of the
 115 farm in which each turbine is placed) is approximately the same as the mean velocity across
 116 the entire farm, U_F . We also assume that the head loss across the entire farm area, H_F , is
 117 much smaller than the average water depth in the farm area (say, less than a few percent of
 118 the average water depth, which is usually the case unless the Froude number of the flow is
 119 very high) and is (again at least approximately) uniform in the cross-stream direction. These
 120 assumptions need to be confirmed in coastal-scale simulations (based on the depth-averaged

121 shallow water equations), where the effect of the farm may be modelled as an additional
122 resistance (by increasing the bed friction coefficient, for example, although we might also
123 need to consider the effect of additional turbulence generated by the turbines on the mixing of
124 flow downstream of the farm area for better accuracy).

125 The purpose of the coastal-scale simulation here is *not* the prediction of the
126 performance (power) of the farm but the assessment of coastal-dynamic characteristics of a
127 given farm site. Specifically, we should obtain from coastal-scale simulations (by varying
128 the flow resistance in the farm area) the *reduction* of the farm-averaged velocity, ΔU_F , as a
129 function of the *increase* in head loss across the farm, ΔH_F . This information, $\Delta U_F = f(\Delta H_F)$,
130 can be used for device-scale simulations to account for the effect of coastal dynamics (i.e.
131 how much the current through the farm should decrease relative to the increase in the head
132 loss) either rigorously as special inlet and outlet boundary conditions (interactively updated
133 during each simulation) or only approximately as a scaling factor in the post-processing of
134 the simulations (by assuming the Reynolds number independence of the flow). In this study
135 we employ the latter approach, which will be demonstrated later in Section 4.

136 It should be noted that there are two extreme scenarios for the changes of U_F and H_F
137 as the flow resistance in the farm area increases: (i) U_F is fixed whereas H_F increases; and (ii)
138 H_F is fixed whereas U_F decreases. The first case is the ‘fixed inflow’ case, which is often
139 assumed in studies focusing on device performance but is physically incorrect. The second
140 case is the ‘fixed head’ case, which is again physically incorrect. Generally the changes of
141 U_F and H_F must lie between the two cases, i.e. U_F somewhat decreases whilst H_F somewhat
142 increases, depending on the coastal dynamics for that particular farm site. The smaller the
143 decrease in U_F (relative to the increase in H_F), the higher the power-generation potential in
144 that area (for a given natural current speed). Hence the purpose of the coastal-scale
145 simulation is, essentially, to select a high power-generation potential site (by assessing not
146 only the natural current speed but also the relationship between ΔU_F and ΔH_F), whereas the
147 device-scale simulation is to examine how to make the most of the potential in that area.

148

149 **3. LES of periodic open channel flow as a part of the two-scale modelling**

150 In this section we present LES of periodic open channel flow (with a porous plate model
151 representing turbines) as an example of the device-scale part of the two-scale modelling of
152 marine turbine arrays. In this study we do not perform any coastal-scale simulations but
153 assume that we have assessed the characteristics of some hypothetical farm sites, described

154 by the form of $\Delta U_F = f(\Delta H_F)$. The effect of such farm-site characteristics on the performance
155 and energetics of marine turbine arrays will be discussed later in Section 4.

156

157 *3.1. Hypothetical farm configuration*

158 In this study we consider a large farm consisting of multiple rows of turbines (often referred
159 to as ‘turbine fences’) as illustrated earlier in Fig. 1. As an example, we consider turbines of
160 the size of 20 metres arrayed regularly (with a lateral spacing of 20 metres between each
161 turbine) within a three-kilometre-square farm area; each row or fence may therefore consist
162 of up to 75 turbines. Here we presume that the streamwise spacing between each fence is
163 large enough (relative to the size of each turbine) so that turbines in a downstream fence are
164 not affected by the wake of individual turbines in upstream fences (the importance of this
165 spacing will be discussed later). If we assume that this spacing needs to be at least 30 times
166 larger than the turbine size, we may install up to six fences in this three-kilometre-square
167 farm area.

168 It should be noted that this spacing between each fence ($20\text{m} \times 30 = 600\text{m}$) is still
169 much shorter than the fence width (3km). Hence we can expect that the local flow condition
170 is nearly the same for most of the turbines in this farm area, which means that the two-scale
171 modelling approach is approximately applicable to this type of farm. Strictly speaking, the
172 flow through the farm area may somewhat decrease downstream (i.e. more flow may go
173 through upstream fences than downstream fences) due to the leakage of flow through the
174 spanwise ends of the farm area (unless the spacing between each fence is negligibly small
175 compared to the fence width). A possible approach to account for the effect of such flow
176 reduction through multiple fences has been reported in [12] but this is not considered in the
177 present study.¹

178

179 *3.2. Computational domain and conditions*

180 Figure 2 describes the computational domain for LES, which represents a (very small) part of
181 the entire farm area. The depth, width and length of the domain are H , $4.8H$ and $12H$,
182 respectively. Cartesian coordinates (x, y, z) are employed to represent the streamwise (x) ,

¹ Neglecting the non-uniformity of (locally-averaged) current speed within the farm area is expected to result in an underestimation of the farm output, essentially because the integral (over the farm area) of the cube of the actual (non-uniform) current speed is larger than that of the averaged (uniform) current speed U_F .

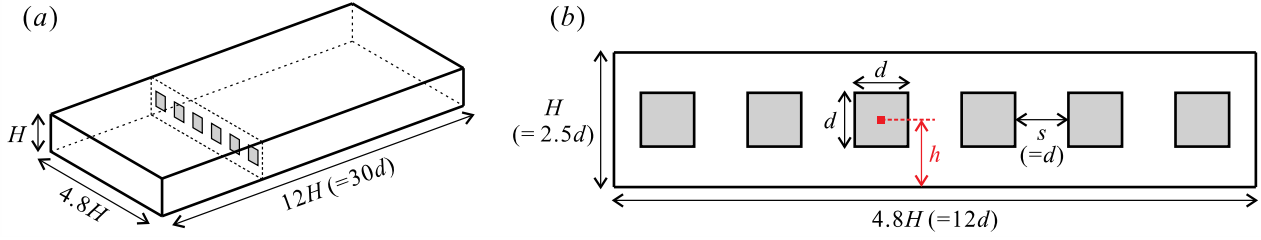


Fig. 2. Computational domain for LES of simplified marine turbines in a periodic open channel: (a) overview of the domain; (b) configuration of the array of turbines.

183 vertical (y) and spanwise (z) directions. Each turbine is modelled as a porous plate, which is
 184 practically the same as the actuator disk model used earlier in [9] (except that the shape of the
 185 plate in this study is square rather than circular). The size of each plate, d , is 40% of the
 186 water depth and six plates are arrayed equidistantly (with spacing $s = d$) across the entire
 187 domain width. The ‘hub-height’ (the distance from the seabed to the centre of each turbine),
 188 h , is varied between 30% and 70% of the water depth H in this study.

189 Here the blockage ratio $B = 0.2$ is the ratio of the total device area ($6d^2$) to the cross-
 190 sectional area of the domain ($30d^2$), whereas the device-to-bed area ratio $R = 0.01667$ is the
 191 ratio of the total device area to the bed area of the domain ($360d^2$). Note that, although not
 192 examined in this study due to the limitation of computational resources, both B and R are
 193 expected to be important for the performance of multiple rows of turbines.

194 One important aspect of the two-scale modelling in this study is that, for the device-
 195 scale simulation, we fix the mass flow through the domain and employ streamwise as well as
 196 spanwise periodic boundary conditions. We also employ the so-called ‘rigid lid’ boundary
 197 conditions for the sea surface, which means that we neglect the effect of local water height
 198 change within this small part of the farm on the performance of individual devices² (although
 199 we do obtain, as an important output of the simulation, the pressure difference between the
 200 inlet and outlet of this kinematically periodic domain). Therefore, for the device-scale
 201 simulation, the only independent flow parameter (apart from the configuration and resistance
 202 of the turbines) is the channel Reynolds number, $Re = \rho U_{\text{ref}} H / \mu$, where μ and ρ are the
 203 viscosity and density of the water, respectively, and U_{ref} is the reference velocity (streamwise
 204 velocity averaged across the cross-section of the computational domain).

² Earlier studies have suggested that this is a reasonable assumption unless the local blockage ratio is extremely high [13].

205 In order to simulate directly a full-scale device flow ($d = 20\text{m}$, $H = 50\text{m}$ and $U_{\text{ref}} =$
206 2m/s , for example) we would need to perform LES of a very high Re ($\sim 10^8$) channel flow,
207 which is computationally too expensive unless some forms of ‘wall functions’ are employed
208 to model empirically the flow near the seabed. Instead of using such wall functions (which
209 would not be very reliable when a strong streamwise pressure gradient is imposed by the
210 turbines/plates), we perform LES at an only moderately high Re of 10935 (with no-slip
211 conditions applied at the seabed) and assume that this Re is high enough to neglect the
212 Reynolds number dependency of this device-scale flow. This assumption can be justified, at
213 least partly, since at this Reynolds number our device models (porous plates) are still located
214 entirely within the so-called ‘outer layer’ (i.e. $y^+ > 50$) where direct effects of viscosity on
215 mean velocity profiles are negligible [14]. Also note that the device model used in this study
216 is a simple porous plate (or actuator disk) model, which does not account for any Reynolds
217 number effects on the device characteristics. Hence the results of the current LES at $\text{Re} =$
218 10935 (to be presented in Section 3.4) will be interpreted as an approximate representation of
219 the device-scale flow at any practical channel Reynolds numbers ($\sim 10^8$) when discussing the
220 performance and energetics of hypothetical farms later in Section 4.

221

222 3.3. Further details of the computations

223 The LES computations were performed using ANSYS FLUENT (v14). The Smagorinsky
224 eddy-viscosity model (with the model coefficient $C_s = 0.065$, following the open channel
225 LES study of Hinterberger et al. [15]) was used to model subgrid-scale stresses. Uniform
226 structured grids with 300 and 240 cells were used in the x and z directions, resulting in
227 resolutions of $\Delta x^+ \approx 24$ and $\Delta z^+ \approx 12$ in wall units, whereas in the y direction 60 cells were
228 used; 45 of which were uniformly allocated at $0.1 \leq y/H \leq 1$ and the other 15 were used to
229 resolve the near-bottom region ($0 \leq y/H \leq 0.1$) with the minimum cell size of $\Delta y^+ \approx 1.2$ at the
230 bottom. A second-order central difference scheme was used for spatial discretisation and a
231 second-order implicit scheme was used for time integration. A constant non-dimensional
232 time step of $U_{\text{ref}} \Delta t/H = 0.04$ was employed throughout the study. The computations were
233 performed for 3000 time steps ($U_{\text{ref}} t/H = 120$, i.e. 10 flow-through time for the periodic
234 domain of $12H$ length) first to obtain a statistically steady flow field, and then for another
235 3000 time steps to obtain statistics of the flow field.

236 The LES computations were performed first for the case without any turbines to
237 compare the results with the open channel LES of Hinterberger et al. [15] at the same channel

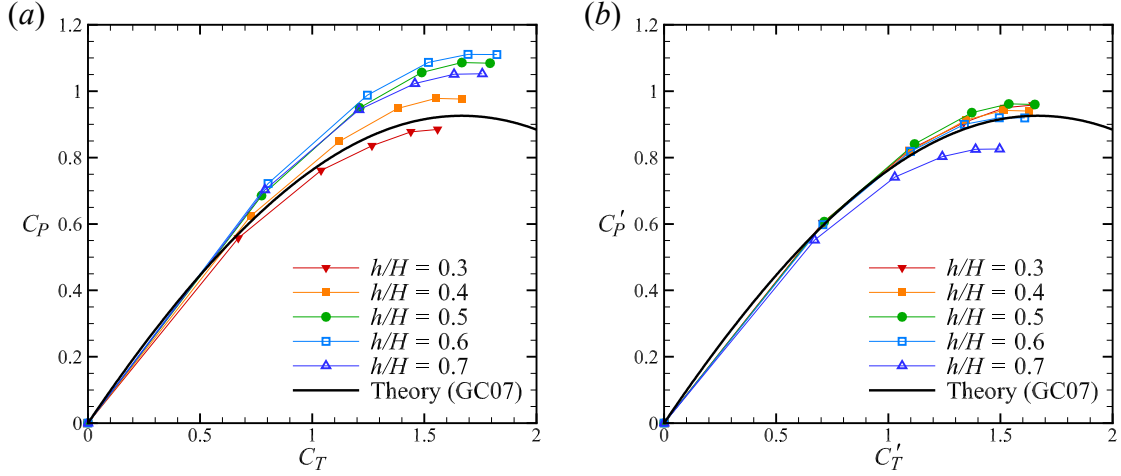


Fig. 3. Mean thrust and power coefficients: (a) original definitions; (b) modified definitions.

238 Reynolds number of 10935 for validation. The skin friction coefficient $C_{f0} = \tau_{w0} / (\frac{1}{2}\rho U_{\text{ref}}^2)$
 239 obtained was 0.00589, which agreed reasonably well with the value 0.00578 from [15] and
 240 also with the value 0.00582 from the direct numerical simulation of (closed rather than open)
 241 channel flow by Moser et al. [16]. Although not shown here for brevity, mean streamwise
 242 velocity and Reynolds stress profiles obtained in this validation case also agreed reasonably
 243 well with those from [15].

244

245 3.4. Results

246 Figure 3(a) shows thrust and power coefficients of the devices (porous plates) obtained for
 247 five different hub-height cases ($h/H = 0.3, 0.4, 0.5, 0.6, 0.7$). Plotted together is the solution
 248 of the analytical model of Garrett and Cummins [5] (hereafter GC07) for the same blockage
 249 $B = 0.2$. As with [9], the thrust and power coefficients, C_T and C_P , are calculated as

$$250 \quad C_T = \frac{[\text{device thrust}]}{\frac{1}{2}\rho U_{\text{ref}}^2 \times [\text{device area}]} = K \frac{\langle U_d^2 \rangle}{U_{\text{ref}}^2} \quad (1)$$

$$251 \quad C_P = \frac{[\text{power extracted}]}{\frac{1}{2}\rho U_{\text{ref}}^3 \times [\text{device area}]} = K \frac{\langle U_d^3 \rangle}{U_{\text{ref}}^3} \quad (2)$$

252 where K is the momentum loss factor (or ‘resistance coefficient’ of porous plates [7]); in this
 253 study we tested five different values ($K = 1, 2, 3, 4$ and 5) for each hub-height case to change
 254 the thrust (note that $K = 2$ is a theoretically optimum value yielding the well-known Betz
 255 limit of $C_P = 0.593$ for an unconfined flow case, but for this confined flow case the optimum

256 value is much larger than 2). U_d is the time-averaged local streamwise velocity at the devices
 257 (porous plates), and $\langle U_d^2 \rangle$ and $\langle U_d^3 \rangle$ are the face averages of U_d^2 and U_d^3 over the device area,
 258 respectively.

259 As can be seen from Fig. 3(a), the maximum C_p increases as h/H increases from 0.3
 260 to 0.6 but then somewhat decreases for $h/H = 0.7$. The increase in C_p for $h/H = 0.3$ to 0.6 is
 261 due to the channel flow being faster at a higher position. This can be confirmed in Fig. 3(b),
 262 which plots modified thrust and power coefficients, C'_T and C'_P , defined based on the square
 263 and cube of the undisturbed channel flow velocity averaged only across the turbine area for
 264 each hub-height case (rather than based on the square and cube of U_{ref} as in Eqs (1) and (2)).
 265 Note that the C'_T versus C'_P curves for $h/H = 0.3, 0.4, 0.5$ and 0.6 are nearly identical, and
 266 that they also agree well with the solution of the GC07 model.

267 Figure 3(b) also shows that the maximum C'_P for $h/H = 0.7$ is about 10% lower than
 268 that for the other cases. The reason for this discrepancy is that, for this particular case, the
 269 mixing of device wake is rather slow and the streamwise gap between the turbine fences ($30d$
 270 in this study, due to the periodic boundary conditions) is not large enough for the wake to
 271 fully recover before reaching the turbines downstream. This can be seen from Figs 4 and 5,
 272 which show mean streamwise velocity profiles along the device centreline and across the
 273 water depth, respectively, for $h/H = 0.3, 0.5$ and 0.7 . In Fig. 4 the results are shown for
 274 moderate ($K = 2$) and high ($K = 4$) resistance cases for each h/H , whereas in Fig. 5 the results
 275 are shown only for the moderate resistance case for each h/H . Note that U_0 used in Fig. 4 is
 276 the undisturbed mean streamwise velocity at each hub-height.

277 As noted earlier in the introduction, one potentially important issue for the design of
 278 marine turbine arrays is how the array configuration affects the bed friction coefficient for the
 279 entire farm area. Here we define the (average) bed friction coefficient as

$$280 \quad \langle C_f \rangle = \frac{\langle \tau_w \rangle}{\frac{1}{2} \rho U_{\text{ref}}^2} \quad (3)$$

281 where $\langle \tau_w \rangle$ is the wall shear stress averaged over the bottom wall of the entire computational
 282 domain. If the bed friction coefficient is higher for a certain array configuration, then more
 283 power tends to be lost/dissipated for this array configuration (as if some rocks, obstacles or
 284 additional device-supporting structures were brought into the farm area). Figure 6(a) shows
 285 the obtained friction coefficient $\langle C_f \rangle$ normalised by that for the case with no turbine thrust,

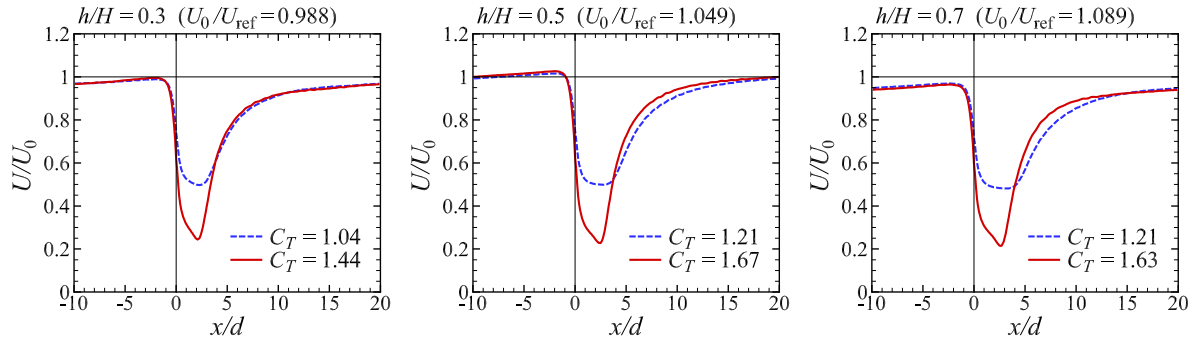


Fig. 4. Mean streamwise velocity along the device centreline: for $h/H = 0.3, 0.5$ and 0.7 . Dashed and solid lines show the results of moderate ($K = 2$) and high ($K = 4$) resistance cases, respectively.

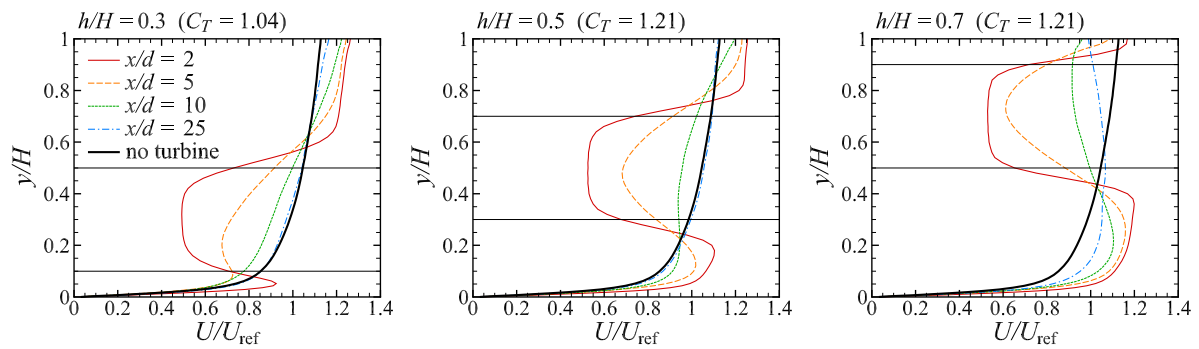


Fig. 5. Mean streamwise velocity profiles across the water depth downstream of the centre of each device (at $x/d = 2, 5, 10$ and 25) for moderate ($K = 2$) resistance cases: for $h/H = 0.3, 0.5$ and 0.7 .

286 $C_{f0} = 0.00589$, for the five different h/H cases. Note that, although the Reynolds number for
 287 the present LES is about four orders-of-magnitude smaller than that for a full-scale device
 288 flow, this C_{f0} value is still in the same order-of-magnitude as that for a full-scale device flow
 289 with some roughness on the seabed (typically between 0.004 and 0.02). As can be seen from
 290 the figure, the friction coefficient was found to increase by up to about 30 ~ 40% as the
 291 turbine thrust was increased, and the rate of increase was found to depend (albeit moderately)
 292 on the hub-height of the turbines (highest for $h/H = 0.7$ and lowest for $h/H = 0.5$).

293 It should be noted, however, that the increase in the bed friction coefficient is not
 294 spatially uniform. Figure 7 shows contours of instantaneous and time-averaged values of the
 295 friction coefficients for $h/H = 0.3, 0.5$ and 0.7 (with $K = 2$). For $h/H = 0.3$, the friction
 296 coefficient is locally very high immediately downstream of the device location ($x/d = 0$). As
 297 h/H is increased to 0.5 and 0.7, this local peak value gradually decreases. For $h/H = 0.7$,
 298 however, the friction level is high in the far downstream region ($x/d > 15$ and $x/d < 0$)
 299 compared to the other two cases. These differences in the spatial variation of C_f suggest that

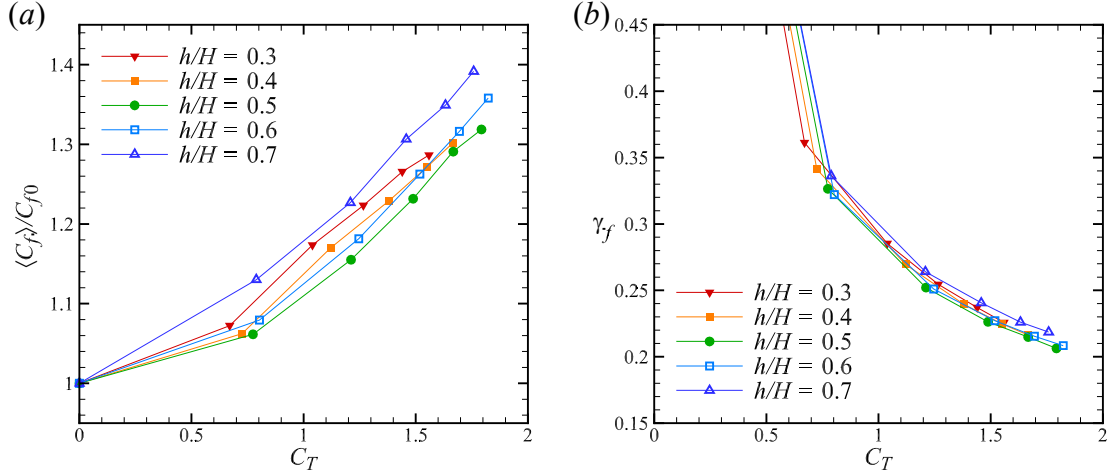


Fig. 6. Effects of turbine thrust on: (a) normalised bed friction coefficient averaged across the entire channel, and (b) the ratio of the bed friction drag to the total drag.

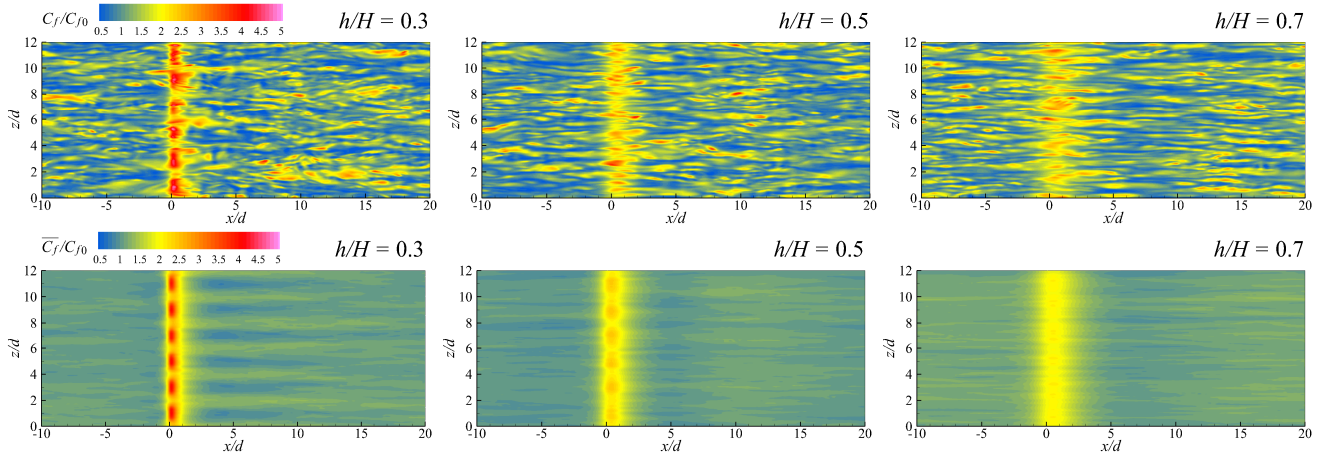


Fig. 7. Contours of skin friction on the bottom of the channel: (top) instantaneous and (bottom) time-averaged results for moderate ($K = 2$) resistance cases, for $h/H = 0.3, 0.5$ and 0.7 .

300 the order of different hub-height cases for the rate of increase in $\langle C_f \rangle$, shown in Fig. 6(a),
 301 might change depending on the streamwise spacing between the turbine fences (or on the
 302 device-to-bed area ratio R). It should also be noted that the porous plate model used in this
 303 study is very simple and might not have simulated accurately the effect of turbine arrays on
 304 the bed friction coefficient. It would therefore be informative to perform a further analysis
 305 on the bed friction coefficient using a more sophisticated turbine model, such as an actuator
 306 line model (e.g. [17]), in future studies.

307 Also of importance is that, although the bed friction coefficient $\langle C_f \rangle$ increases with
 308 the turbines' thrust coefficient C_T as shown earlier in Fig. 6(a), this increase in $\langle C_f \rangle$ is (at

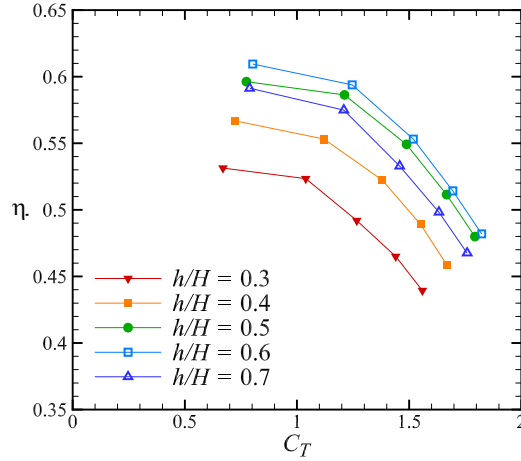


Fig. 8. Effect of turbine thrust on the energy conversion efficiency of the device array.

309 least in the present study using the porous plate model) rather gentle relative to the increase
 310 of the turbine thrust. Figure 6(b) presents the ratio of the bed friction drag to the total drag, γ_f ,
 311 which is calculated by

$$312 \quad \gamma_f = \frac{[\text{bed friction drag}]}{[\text{total drag}]} = \frac{\langle C_f \rangle}{\langle C_f \rangle + RC_T} \quad (4)$$

313 where R ($= 0.01667$ in this study) is the device-to-bed area ratio defined earlier in Section 3.2.
 314 It can be seen that this ratio decreases down to about 0.2 as C_T increases, i.e. the bed friction
 315 drag accounts for only about 20% of the total drag for high thrust cases simulated in this
 316 study. This essentially means that, as will be shown later in Section 4, the power loss due to
 317 seabed friction becomes less important (compared to that due to device wake mixing) as the
 318 turbine thrust increases.

319 Finally, Fig. 8 shows the effect of turbine thrust on the energy conversion efficiency
 320 (sometimes referred to as ‘basin efficiency’) of the device array:

$$321 \quad \eta = \frac{[\text{power extracted}]}{[\text{power removed from the flow}]} = \frac{RC_P}{\langle C_f \rangle + RC_T} \quad (5)$$

322 As can be seen from the above equation, the efficiency is zero when C_T is zero (since C_P is
 323 zero whilst $\langle C_f \rangle$ is non-zero). However the efficiency increases very rapidly (up to about
 324 0.6, depending on h/H) as C_T and C_P increase from zero to non-zero values, and then
 325 decreases gradually as C_T further increases. For the sake of convenience, here we can also

326 define another type of power coefficient representing the power removed from the flow (i.e.
 327 sum of that extracted as useful power and that dissipated into heat):

$$328 \quad C_{P+} = \frac{[\text{power removed from the flow}]}{\frac{1}{2} \rho U_{\text{ref}}^3 \times [\text{device area}]} = \frac{C_P}{\eta} \quad (6)$$

329 As will be shown later in Section 4, the energy conversion efficiency η , or alternatively C_{P+} ,
 330 is important for understanding the performance and energetics of large marine turbine arrays
 331 that cause the reduction of flow through the entire farm area.

332

333 **4. Energetics of marine turbine arrays**

334 In the following we demonstrate how the results of device-scale simulations can be used to
 335 assess the performance and energetics of multiple rows of devices deployed at a given farm
 336 site. As described earlier, the basic idea underlying the two-scale coupling in this study is
 337 that we assume the Reynolds number independence of device-scale flow dynamics, so that
 338 the LES results presented earlier (namely C_P , C_T and $\langle C_f \rangle$) obtained for various h/H and K)
 339 represent those at any practical Reynolds numbers ($10^7 \sim 10^8$). Specifically, here we assume
 340 that the same LES results (C_P , C_T and $\langle C_f \rangle$) for given h/H and K) are obtained for the
 341 following dimensional parameters: $d = 20\text{m}$, $H = 50\text{m}$ and $U_{\text{ref}} = U_F = 1 \sim 2\text{m/s}$. Note that a
 342 natural interpretation of H is the average water depth for the entire farm area, although this
 343 may alternatively be interpreted as a local water depth in any part of the farm, provided that
 344 the total head loss across the farm (H_F) is always much smaller than this water depth (even
 345 for high turbine-thrust cases). Meanwhile, the mean current velocity across the farm (U_F)
 346 may reduce significantly from that for the zero turbine-thrust case, U_{F0} ($= 2\text{m/s}$).

347 As already mentioned briefly in Section 2, we define ΔU_F as the reduction of U_F and
 348 ΔH_F as the increase of H_F (compared to the zero turbine-thrust case); hence the following
 349 relationships exist:

$$350 \quad U_F = (U_{F0} - \Delta U_F) \quad (7)$$

$$351 \quad H_F = (H_{F0} + \Delta H_F) \ll H \quad (8)$$

352 where H_{F0} is the value of head loss H_F for the zero turbine-thrust case. Here we consider
 353 deriving the relationship between U_F and H_F from the results of device-scale simulations first.
 354 Although the effect of local water height change was neglected in our LES employing the

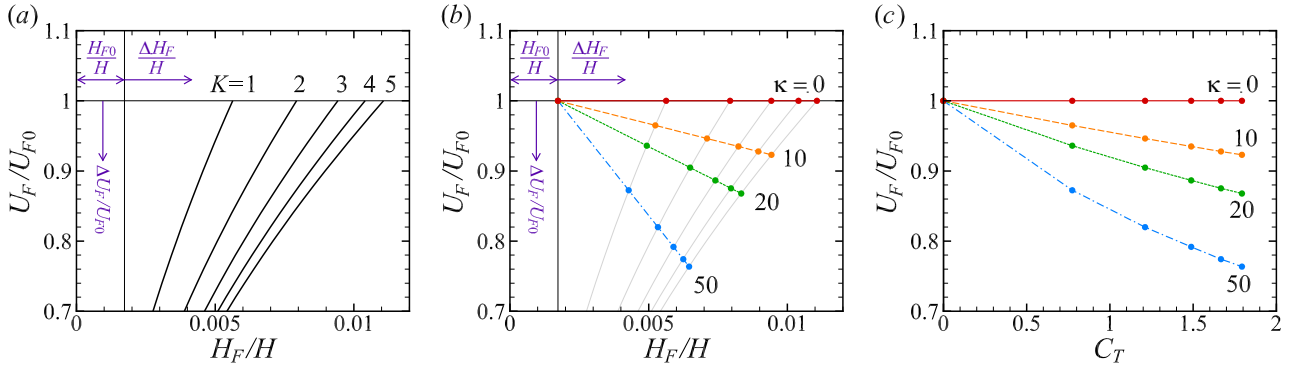


Fig. 9. Two-scale coupling process to determine the farm flow reduction for four hypothetical farm sites ($\kappa = 0, 10, 20$ and 50), for $h/H = 0.5$ and $n_{\text{row}} = 6$: (a) U_F vs. H_F obtained from the device-scale problem (i.e. solutions of Eq. (12)) for $K = 1, 2, 3, 4$ and 5 ; (b) U_F vs. H_F obtained from the coastal-scale problem (i.e. solutions of Eq. (14)); and (c) determined farm flow velocities plotted against C_T .

355 ‘rigid lid’ assumption, we can still estimate the total head loss across the farm (H_F) from the
 356 pressure loss between the inlet and outlet of the LES computational domain, $P_{\text{in}} - P_{\text{out}}$,
 357 multiplied by the number of turbine rows in the farm, n_{row} , as

$$358 \quad H_F = n_{\text{row}} \left(\frac{P_{\text{in}} - P_{\text{out}}}{\rho g} \right) \quad (9)$$

359 where $g = 9.8\text{m/s}^2$ is the acceleration due to gravity. Here the pressure loss can be calculated
 360 for a given U_F (by considering the momentum conservation within the LES domain and also
 361 the Reynolds number independence of $\langle C_f \rangle$ and C_T) as

$$362 \quad P_{\text{in}} - P_{\text{out}} = \frac{1}{2} \rho U_F^2 \frac{B}{R} (\langle C_f \rangle + RC_T) \quad (10)$$

363 and hence, from Eqs (9) and (10), we obtain

$$364 \quad H_F = \frac{n_{\text{row}}}{2} \frac{U_F^2}{g} \frac{B}{R} (\langle C_f \rangle + RC_T) \quad (11)$$

365 or alternatively

$$366 \quad \frac{H_F}{H} = \frac{n_{\text{row}}}{2} (\text{Fr}_0)^2 \frac{B}{R} (\langle C_f \rangle + RC_T) \left(\frac{U_F}{U_{F0}} \right)^2 \quad (12)$$

367 where $\text{Fr}_0 = U_{F0} / \sqrt{gH} = 0.0904$ is the Froude number of the flow for the case with no turbine
 368 thrust. As an example, Fig. 9(a) shows solutions of Eq. (12) obtained for the medium hub-

369 height case $h/H = 0.5$ (with five different device conditions, $K = 1, 2, 3, 4, 5$) and $n_{\text{row}} = 6$.
 370 Note that we can also calculate H_{F0} from Eq. (12) by considering $\langle C_f \rangle = C_{f0}$, $C_T = 0$ and
 371 $U_F/U_{F0} = 1$.

372 Meanwhile, the relationship between U_F and H_F can be obtained from coastal-scale
 373 simulations as well, as mentioned earlier in Section 2. For demonstration purposes, here we
 374 consider that the relationship between ΔU_F and ΔH_F can be approximated (when ΔU_F is not
 375 very large, say $\Delta U_F/U_{F0} < 0.3$) by the following linear function:

$$376 \quad \frac{\Delta U_F}{U_{F0}} = \kappa \frac{\Delta H_F}{H} \quad (13)$$

377 where κ is a site-specific parameter describing how much the flow through the entire farm
 378 tends to reduce relative to the increase in the head loss across the farm (note that $\kappa = 0$ and ∞
 379 correspond to the ideal ‘fixed inflow’ and ‘fixed head’ scenarios, respectively). Hence, by
 380 substituting Eqs (7) and (8), we obtain

$$381 \quad \frac{U_F}{U_{F0}} = 1 - \kappa \left(\frac{H_F}{H} - \frac{H_{F0}}{H} \right). \quad (14)$$

382 Figure 9(b) shows solutions of Eq. (14) for four different hypothetical farm sites with $\kappa = 0$,
 383 10, 20 and 50. Plotted together in this figure (with light gray lines) are the solutions of Eq.
 384 (12) shown earlier in Fig. 9(a). Since both Eqs (12) and (14) must be satisfied, these are the
 385 two equations to be solved simultaneously to determine U_F and H_F (as indicated by symbols
 386 in Fig. 9(b)) for a given set of device-scale and coastal-scale conditions (array configuration,
 387 operating conditions of devices and farm-site characteristics). The determined U_F values (for
 388 the four hypothetical farm sites) are re-plotted against the devices’ thrust coefficient in Fig.
 389 9(c), showing the importance of farm-site characteristics (represented by κ) on the reduction
 390 of flow through the entire farm area.

391 As the farm flow reduction has been determined successfully by coupling the device-
 392 scale and coastal-scale problems, we can now analyse the overall energetics (energy budgets)
 393 of turbine arrays as a farm. For the sake of convenience, here we introduce the farm flow
 394 reduction factor:

$$395 \quad \alpha = \frac{U_F}{U_{F0}} \quad (15)$$

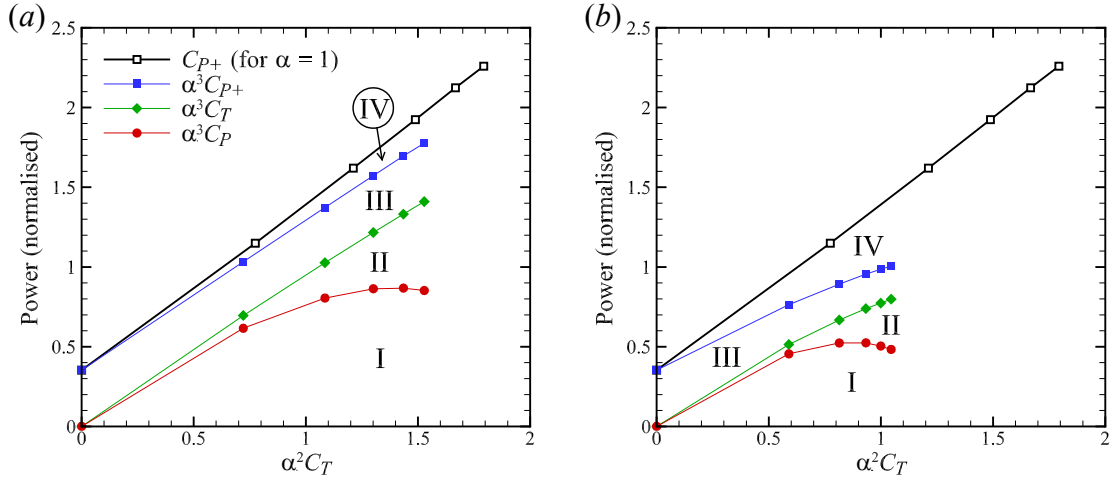


Fig. 10. Energetics of marine turbine arrays installed in: (a) high potential ($\kappa = 10$) and (b) low potential ($\kappa = 50$) farm sites, for $h/H = 0.5$ and $n_{\text{row}} = 6$. The meanings of Regions I to IV are as follows. I: power extracted as useful power, II: power dissipated due to device wake mixing, III: power dissipated due to bed-induced shear, and IV: diminution of the total power removed from the farm area due to the reduction of flow through the farm.

396 so that the ‘global’ thrust and power coefficients of devices deployed in the farm (i.e. the
 397 coefficients defined using the undisturbed current speed U_{F0} rather than U_F) are $\alpha^2 C_T$ and
 398 $\alpha^3 C_P$, respectively, in analogy with those defined in [8, 9]. Also, the ‘global’ version of C_{P+}
 399 defined earlier in Eq. (6) is now described as $\alpha^3 C_{P+}$. Note that both $\alpha^3 C_P$ and $\alpha^3 C_{P+}$ may
 400 represent power (extracted or removed) for either one device or all devices, relative to the
 401 kinetic power of undisturbed flow through the *corresponding* device area (i.e. area for one
 402 device or all devices). In addition, since $C_{P+} = C_T$ when the bed friction loss is zero (note
 403 that $\eta = C_P/C_T$ when $\langle C_f \rangle = 0$), we can consider $\alpha^3 C_T$ to represent the sum of the power
 404 extracted as useful power and that lost due to device wake mixing (again relative to the
 405 kinetic power of undisturbed flow through the corresponding device area).

406 Two examples of the energetics of turbine arrays, deployed as a farm in high ($\kappa = 10$)
 407 and low ($\kappa = 50$) potential sites, are presented in Fig. 10 (for $h/H = 0.5$, $n_{\text{row}} = 6$). Note that
 408 the vertical axis shows power (for either one device or all devices) normalised by the kinetic
 409 power of undisturbed flow through the corresponding device area, whilst the horizontal axis
 410 shows the global thrust coefficient of devices. Here we can consider four different factors
 411 contributing to the energetics of device arrays, namely Regions I to IV denoted in Fig. 10:
 412 Region I represents the power extracted as useful power, Region II is the power dissipated
 413 due to device wake mixing, Region III is the power dissipated due to bed-induced shear, and

414 Region IV is the diminution of the total power removed from the farm area due to the farm
415 flow reduction (compared to the case where the flow through the farm does not reduce at all,
416 i.e. $\alpha = 1$, for any device thrust conditions). As can be seen from the figure, the diminution of
417 the power removed from the farm (Region IV) is small when the devices are deployed in the
418 high potential farm site ($\kappa = 10$), but this increases significantly in the low potential farm site
419 ($\kappa = 50$). Of importance here is that, as κ increases and thus Region IV increases, Regions I
420 to III diminish all together, i.e. the power extracted as useful power and that dissipated into
421 heat both decrease, since they are all proportional to α^3 . As a result, the optimal operating
422 condition (or thrust condition) of devices to maximise the output power (Region I) changes
423 significantly depending on the value of κ or the farm-site characteristics.

424 Finally, it should be remembered that, since we employed an ideal porous plate (or
425 actuator disk) model to simulate the effect of devices, the ‘extracted’ power (Region I) here
426 represents the *limit* of power extraction. For actual marine turbines, some of this ‘extracted’
427 power (Region I) would not be extracted but be wasted, either (i) by generating heat at the
428 turbines due to mechanical losses etc., or (ii) by generating additional fluid motions, such as
429 mean swirling, large-scale coherent motions and turbulence (sometimes referred to as blade-
430 induced turbulence or BIT [18]), the power of which is also eventually dissipated into heat
431 due to additional wake mixing [19]. Such additional loss may also be caused due to device-
432 supporting structures. It would therefore be useful to perform a similar two-scale analysis
433 using a more practical turbine model in future studies. Also note that the diminution of the
434 power removed from the farm (Region IV) can be due to two different types of reduction of
435 flow through the farm, depending on how large the drag caused by the farm is compared to
436 the driving force of the ocean current. If the farm drag is negligibly small compared to the
437 driving force (which is usually the case), the farm flow reduction is essentially due to very-
438 large-scale flow deflection (as illustrated in Fig. 1), which generally results in additional
439 mixing and thus an increase in dissipation somewhere outside of the farm. However, if the
440 farm is extremely large and the farm drag is not negligibly small compared to the driving
441 force, the farm would somewhat decelerate the ocean current and therefore the flow through
442 the farm may reduce even without any flow deflection around the farm.

443

444 **5. Conclusions**

445 In this study we discussed a generic two-scale modelling approach to understand/predict the
446 performance and energetics of a large number (more than a few hundred) of marine turbines

447 forming a hydro-power farm in a general coastal environment. Similarly to the theoretical
448 partial tidal fence model recently proposed in [8], this approach consists of two individual
449 parts (simulations) of different scales, namely the device-scale and coastal-scale simulations.
450 The purpose of the coastal-scale simulation is not the prediction of the performance (output
451 power) of the farm but to assess the reduction of flow through the farm as a function of the
452 increase of head loss across the farm. This information is used to account for the so-called
453 coastal dynamics effects (for that particular farm site) when analysing the results of device-
454 scale simulations (simulating only a small part of the entire farm) to eventually predict the
455 performance and energetics of large turbine arrays deployed as a farm.

456 To demonstrate how the present two-scale modelling approach would work, we have
457 also performed LES of periodic open channel flow over a spanwise array of six devices
458 (represented by porous plate models, with various hub-height) as an example of device-scale
459 simulations, whilst employing a simple model function to account for the coastal dynamics
460 effects for four hypothetical farm sites. Results demonstrated that this approach can be used
461 to study effectively how the energetics of a large number of devices as a farm (i.e. extraction,
462 dissipation and diminution of energy within the entire farm area) may change depending on
463 the farm site characteristics, array configuration (hub-height in this example) and device
464 operating conditions, although the influence of the hub-height was found to be relatively
465 minor in this example. Most importantly, this approach would be very useful to determine
466 the optimal operating (or thrust) condition of a large number of devices to maximise their
467 total output power for a given farm site and for a given array configuration.

468 Finally, it should be noted that this two-scale modelling/analysis is easily applicable
469 to many other device-scale simulations using more practical device models, such as actuator
470 line models and even fully-resolved rotor models with device-supporting structures. Such
471 device-scale simulations coupled with the results of coastal-scale simulations would provide
472 a more practical and reliable prediction of the performance and energetics of marine turbine
473 arrays deployed as a large farm.

474

475 **Acknowledgement**

476 The authors gratefully acknowledge the support of the Oxford Martin School, University of
477 Oxford, who have funded this research.

478

479

480 **References**

- 481 [1] Garrett C, Cummins P. The power potential of tidal currents in channels. *Proceedings of*
482 *the Royal Society A* 2005; **461**: 2563-2572.
- 483 [2] Vennell R. Tuning turbines in a tidal channel. *Journal of Fluid Mechanics* 2010; **663**:
484 253-267.
- 485 [3] Vennell R. Tuning tidal turbines in-concert to maximise farm efficiency. *Journal of*
486 *Fluid Mechanics* 2011; **671**: 587-604.
- 487 [4] Vennell R. The energetics of large tidal turbine arrays. *Renewable Energy* 2012; **48**:
488 210-219.
- 489 [5] Garrett C, Cummins P. The efficiency of a turbine in a tidal channel. *Journal of Fluid*
490 *Mechanics* 2007; **588**: 243-251.
- 491 [6] Housby GT, Draper S, Oldfield MLG. Application of linear momentum actuator disc
492 theory to open channel flow. Tech. Rep. OUEL 2296/08, Dept. Engineering Science,
493 University of Oxford; 2008.
- 494 [7] Whelan JJ, Graham JMR, Peiró J. A free-surface and blockage correction for tidal
495 turbines. *Journal of Fluid Mechanics* 2009; **624**: 281-291.
- 496 [8] Nishino T, Willden RHJ. The efficiency of an array of tidal turbines partially blocking a
497 wide channel. *Journal of Fluid Mechanics* 2012; **708**: 596-606.
- 498 [9] Nishino T, Willden RHJ. Two-scale dynamics of flow past a partial cross-stream array
499 of tidal turbines. *Journal of Fluid Mechanics* 2013; **730**: 220-244.
- 500 [10] Adcock TAA, Draper S, Housby GT, Borthwick AGL, Serhadlioglu S. The available
501 power from tidal stream turbines in the Pentland Firth. *Proceedings of the Royal Society*
502 *A* 2013; **469**: 20130072.
- 503 [11] Nishino T. Beyond the Betz theory – blockage, wake mixing and turbulence. In: *Proc.*
504 *2nd Oxford Tidal Energy Workshop*, Oxford, UK, March 2013, pp. 21-22.
- 505 [12] Draper S, Nishino T. Centred and staggered arrangements of tidal turbines. *Journal of*
506 *Fluid Mechanics* (in press).
- 507 [13] Consul CA, Willden RHJ, McIntosh SC. Blockage effects on the hydrodynamic
508 performance of a marine cross-flow turbine. *Philosophical Transactions of the Royal*
509 *Society A* 2013; **371**: 20120299.
- 510 [14] Pope SB. *Turbulent Flows*. Cambridge University Press, Cambridge, UK; 2000.

- 511 [15] Hinterberger C, Fröhlich J, Rodi W. 2D and 3D turbulent fluctuations in open channel
512 flow with $Re_\tau = 590$ studied by large eddy simulation. *Flow, Turbulence and*
513 *Combustion* 2008; **80**: 225-253.
- 514 [16] Moser RD, Kim J, Mansour NN. Direct numerical simulation of turbulent channel flow
515 up to $Re_\tau = 590$. *Physics of Fluids* 1999; **11**: 943-945.
- 516 [17] Churchfield MJ, Li Y, Moriarty PJ. A large-eddy simulation study of wake propagation
517 and power production in an array of tidal-current turbines. *Philosophical Transactions*
518 *of the Royal Society A* 2013; **371**: 20120421.
- 519 [18] Nishino T, Willden RHJ. Effects of 3-D channel blockage and turbulent wake mixing on
520 the limit of power extraction by tidal turbines. *International Journal of Heat and Fluid*
521 *Flow* 2012; **37**: 123-135.
- 522 [19] Sequeira CL, Miller RJ. Loss mechanisms in tidal stream turbines. In: *Proc. 10th*
523 *European Wave and Tidal Energy Conference (EWTEC 2013)*, Aalborg, Denmark,
524 September 2013.